



Limnology and Oceanography Letters 8, 2023, 760–769
© 2023 The Authors. Limnology and Oceanography Letters published by Wiley Periodicals LLC
on behalf of Association for the Sciences of Limnology and Oceanography.
doi: 10.1002/holz.10342

LETTER

Global Ocean dimethylsulfide photolysis rates quantified with a spectrally and vertically resolved model

Martí Galí , 1* Emmanuel Devred , 2 Gonzalo L. Pérez , 3 David J. Kieber , 4 Rafel Simó .

¹Institut de Ciències del Mar–CSIC, Barcelona, Catalonia, Spain; ²Fisheries and Oceans Canada, Bedford Institute of Oceanography, Dartmouth, Nova Scotia, Canada; ³Instituto INIBIOMA (CRUB Comahue, CONICET), Rio Negro, Argentina; ⁴Department of Chemistry, State University of New York, College of Environmental Science and Forestry, Syracuse, New York, USA

Scientific Significance Statement

Dimethylsulfide (DMS) is a gas produced by marine microbes that, once emitted to the atmosphere, affects the formation of atmospheric particles (aerosols) and clouds, and hence climate. Several processes can remove DMS from the upper ocean layer, therefore controlling DMS emissions. One such process that has not been accurately quantified hitherto is the oxidation of DMS by chemical reactions driven mostly by UV radiation. Using a model that combines satellite observations and in situ data, here we show that DMS photolysis varies across regions and seasons; and quantify global photochemical DMS removal from the surface ocean at around 20 million tons of sulfur per year, 30% less than DMS emission to the atmosphere. Our best estimates are not compatible with estimates from simplified equations for DMS photolysis that are currently used in the numerical models that inform climate projections, stressing the need to improve those models.

Abstract

Photochemical reactions initiated by ultraviolet radiation remove the climate-active gas dimethylsulfide (DMS) from the ocean's surface layer. Here, we quantified DMS photolysis using a satellite-based model that accounts for spectral irradiance attenuation in the water column, its absorption by chromophoric dissolved organic matter, and the apparent quantum yields (AQYs) with which absorbed photons degrade DMS. Models with two alternative parameterizations for AQY estimate global DMS photolysis at between 17 and 20 Tg S yr $^{-1}$, equivalent to 13–15 Tg C yr $^{-1}$, of which \sim 73% occurs in the Southern hemisphere. This asymmetry results mostly from the high AQYs found south of 40° S, which more than counteract the prevailing low irradiance and deep mixing in that region. Simplified schemes currently used in biogeochemical models, whereby photolysis follows the vertical attenuation of visible radiation, overestimate DMS photolysis by around 150% globally. We propose relevant corrections and simple adjustments to those models.

*Correspondence: mgali@icm.csic.es

Associate editor: Claudia Benitez-Nelson

Author Contribution Statement: M.G. conceived the study with initial contributions from R.S. and D.J.K. M.G. coded the photolysis model and ran the radiative transfer and photolysis calculations, processed the input and output datasets, made the figures and wrote the first draft of the manuscript. E.D. and G.L.P. contributed to underwater irradiance modeling. All authors commented on manuscript drafts and contributed to the final version.

Additional Supporting Information may be found in the online version of this article.

This is an open access article under the terms of the Creative Commons Attribution License, which permits use, distribution and reproduction in any medium, provided the original work is properly cited.

The biogenic gas dimethylsulfide (DMS), produced mostly by pelagic microbial food webs, represents the largest natural source of atmospheric sulfur (Hulswar et al. 2022). The products of atmospheric DMS oxidation, chiefly methanesulfonic and sulfuric acids, promote new particle formation and growth, which overall results in planetary cooling through enhanced aerosol light scattering and cloud albedo (Shaw 1983; Charlson et al. 1987; Carslaw et al. 2013). Despite continued efforts to represent DMS-mediated feedbacks in Earth System models, these models do not accurately represent sea-surface DMS concentration fields (Tesdal et al. 2016) and cannot reliably predict future DMS emission trends under global change scenarios (Bock et al. 2021).

DMS is lost from the upper ocean mainly through bacterial consumption, photochemical oxidation and ventilation to the atmosphere. Although bacterial consumption typically accounts for 50–90% of DMS removal (Galí and Simó 2015), all processes can temporarily dominate (Toole et al. 2006; del Valle et al. 2009; Yang et al. 2013; Zhai et al. 2020). Biogeochemical models must capture the variability in these processes to accurately reproduce sea-surface DMS concentration fields, which ultimately control DMS emissions (Tesdal et al. 2016). However, large uncertainties in spatiotemporal DMS distribution remain owing to sparse observations, limited mechanistic understanding and insufficiently validated parameterizations (Le Clainche et al. 2010; Galí and Simó 2015).

DMS photolysis is a photosensitized process, whereby DMS is oxidized by the reactive species generated through the absorption of solar radiation by optically active substances (Brimblecombe and Shooter 1986), mainly chromophoric dissolved organic matter (CDOM; Toole et al. 2003, 2004; Bouillon and Miller 2004; Galí et al. 2016). To quantify the efficiency of this process, an apparent quantum yield (AQY) is computed as the mol DMS oxidized per mol quanta absorbed by CDOM at each wavelength (λ). Typically, AQY decreases exponentially over the solar spectrum. Like other photochemical processes (Fichot and Miller 2010), the spectral product of AQY, CDOM absorption and irradiance produces a peak in DMS photolysis between 320 and 330 nm at the sea surface. The photolysis spectrum progressively shifts toward longer wavelengths as radiation propagates down the water column because shortwave ultraviolet (UV) attenuates faster than longwave UV and visible light. Thus, adequate spectral and vertical resolution are needed for accurate photochemical modeling. Although this has been known for decades, DMS photolysis is still expressed as a function of visible light in biogeochemical models (Chu et al. 2003; Vogt et al. 2010; Belviso et al. 2012).

A global meta-analysis of in situ rates (Galí et al. 2016) found that variability in DMS photolysis AQY at 330 nm, AQY(330), was to first order an inverse function of the corresponding CDOM absorption coefficient, $a_{\rm CDOM}(330)$ (Fig. 1a). Furthermore, four end-member water types were identified: (i) riverinfluenced seawater with abundant terrestrially derived CDOM

and low AQY; (ii) oligotrophic gyre waters with intensely photobleached CDOM, and (iii) productive ocean waters with fresh autochthonous CDOM, both with intermediate AQY; (iv) recently upwelled Southern Ocean waters with potentially old CDOM and high AQY. That study also examined the roles of nitrate and temperature. Although they found a consistent nitrate-dependent increase of AQY(330) across locations, this effect could not account for the tenfold difference in AQY found between subtropical gyre (e.g., Sargasso Sea) and Southern Ocean waters, which have only slightly greater a_{CDOM}(330) but 30 μ M greater nitrate concentration (see Toole et al. 2004). They also found that the enhancing effects of temperature on photolysis kinetics were different across locations and, again, insufficient to explain large-scale AQY variability. Hence, it was concluded that CDOM composition mainly controlled AQYs through yet unknown processes.

Despite these gaps in mechanistic knowledge, Galí et al. (2016) found that nitrate and temperature were the only variables that could statistically explain the AQY variance left after accounting for the dominant $a_{\rm CDOM}(330)$ -driven variance. Building on this work, here we implemented a spectrally and vertically resolved model that uses remotely sensed data to compute DMS photolysis rates in the global ocean. We compared our results to those obtained with two simple parameterizations extracted from prognostic biogeochemical models

Model description and implementation Empirical AOY models

Our spectrally resolved model relies on the empirical estimation of the DMS photolysis AQY at 330 nm and subsequently the AQY spectrum, AQY(λ) (units of s⁻¹ [mol photons m⁻³ s⁻¹]⁻¹ = m³ [mol photons]⁻¹). In the dataset compiled by Galí et al. (2016), AQY(330) data were fitted using two multiple regression models. The first model (*CDOM_NO3*) represents AQY(330) as a function of a_{CDOM}(330) and nitrate concentration [NO₃⁻].

$$\begin{split} log_{10}[AQY(330)] = & -0.4548 - 0.8392 \cdot log_{10}[a_{CDOM}(330)] \\ & + 0.0293[NO_3{}^-] \end{split} \tag{eq1A}$$

The second model ($CDOM_SST$) represents AQY(330) as a function of $a_{CDOM}(330)$ and sea-surface temperature (SST), with a linear interaction term.

$$\begin{split} \log_{10}[\text{AQY}(330)] &= -0.4629 - 1.5774 \cdot \log_{10}[a_{\text{CDOM}}(330)] \\ &+ 0.0049 \cdot \text{SST} + 0.0374 \cdot \log_{10}[a_{\text{CDOM}}(330)] \\ &\cdot \text{SST} \end{split}$$
 (eq1B)

Models *CDOM_NO3* and *CDOM_SST* accounted, respectively, for 84% and 83% of the variance of log₁₀[AQY(330)]

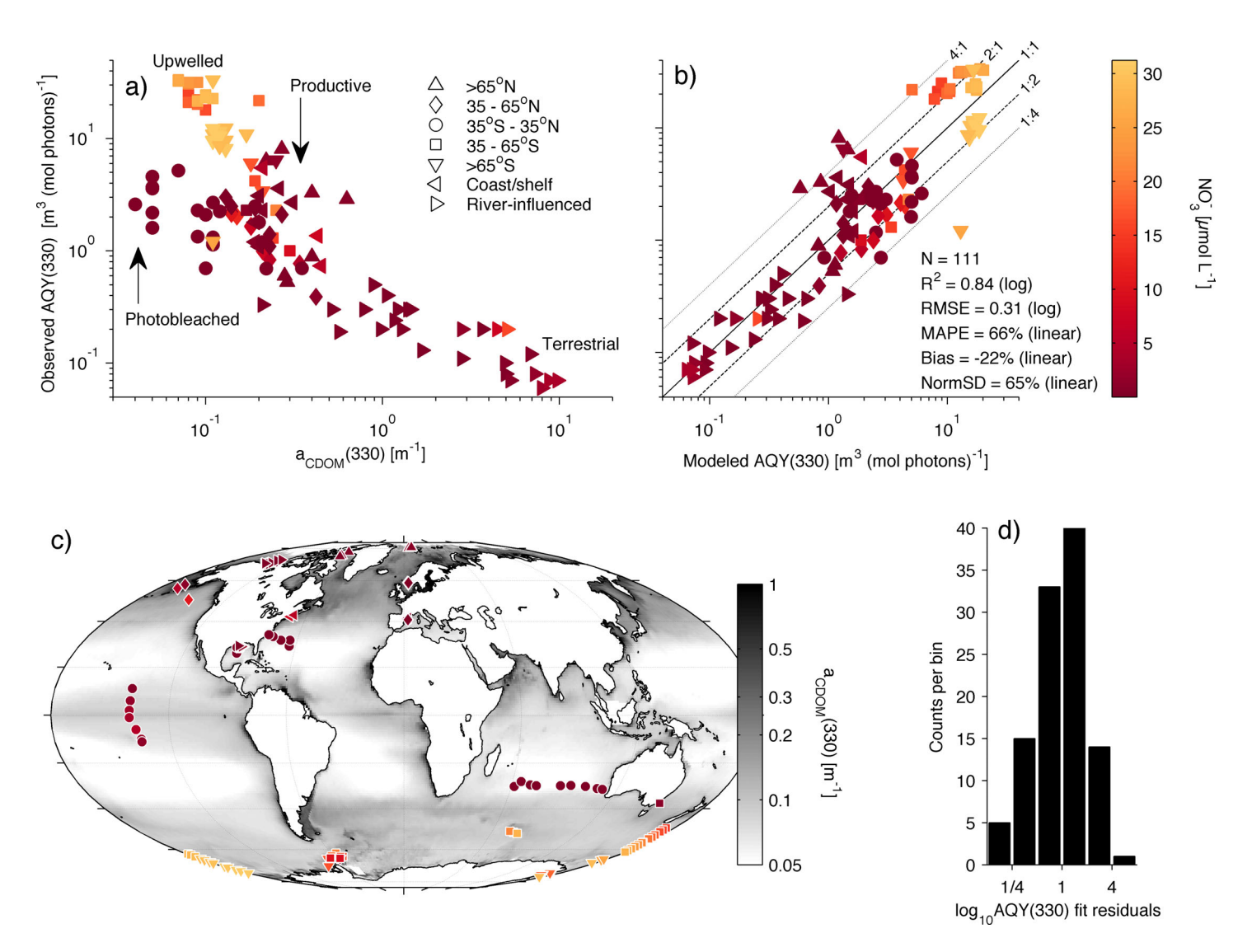


Fig. 1. (a) Relationship between AQY at 330 nm, AQY(330), and the CDOM absorption coefficient, $a_{CDOM}(330)$; (b) comparison between observed AQY(330) and that predicted with an empirical model that uses $a_{CDOM}(330)$ and nitrate as predictors (Eq. 1A); (c) map of the sampling locations overlaid on SeaWiFS-retrieved absorption of chomophoric dissolved organic matter at 330 nm, $a_{CDOM}(330)$; (d) histogram of fit residuals expressed as model/ observations ratio. The color scale in (a) and (b) shows nitrate concentration; symbols are used to distinguish different biogeochemical domains, and labels indicate "end-members" (see text). The black line in (b) shows 1:1 model: data agreement, and the dashed and dotted lines show, respectively, deviations by a factor of 2 and 4 from the 1:1 line. Statistics shown in (b) are the log_{10} -space log_{10} and root-mean-squared error, and the linear-space mean absolute percentage error, mean bias, and normalized standard deviation (values <100% imply underestimation of observed variance).

(n=111) The $CDOM_NO3$ model had slightly better skill metrics (Fig. 1 and Supporting Information Fig. S1) and smaller fit residuals at both extremes of the AQY distribution (Supporting Information Figs. S2 and S3), and is therefore adopted as the reference model. Yet, both AQY(330) models are used in subsequent calculations to better assess AQY-driven uncertainty.

Following Galí et al. (2016), the AQY spectrum was computed from AQY(330) and a spectral slope S_{AQY} such that:

$$AQY(\lambda) = AQY(330) \cdot exp[-S_{AQY} \cdot (\lambda - 330)] \tag{eq2}$$

where S_{AQY} was itself a function of AQY(330) according to a fit that accounted for 29% of its observed variance (n = 47):

$$S_{AOY} = 0.0429 + 0.0147 \cdot \log_{10}[AQY(330)]$$
 (eq3)

Depth-dependent spectrally resolved model

Vertical profiles of the DMS photolysis rate constant, $k_{p,z}$ (d⁻¹), were computed as:

$$k_{p,z} = \int E_{d,0-}(\lambda) \cdot \exp(-K_d(\lambda) \cdot z) \cdot (1/\mu_d) \cdot a_{CDOM}(\lambda) \cdot AQY(\lambda) d\lambda$$
(eq4)

where $E_{d,0-}(\lambda)$ is the downwelling spectral irradiance just below the sea surface (mol photons $m^{-2} d^{-1} nm^{-1}$), $K_d(\lambda)$ is the diffuse vertical attenuation coefficient of downwelling irradiance (m $^{-1}$), μ_d is the mean cosine of underwater irradiance (required to convert planar irradiance to scalar irradiance; unitless), and $a_{CDOM}(\lambda)$ is the CDOM absorption coefficient spectrum (m⁻¹). The spectral terms in Eq. 4 were computed at 5 nm resolution; spectral integration between 290 and 500 nm yielded the photolysis rate constant at a given depth. Along the vertical dimension (z), the model had 39 levels whose spacing increased exponentially from 0.01 m at the surface to 20 m at 100 m. The bottom level was determined by the mixed layer depth (MLD; obtained from Schmidtko et al. (2013)). Mean daily photolysis rate constants in the upper mixed layer (UML), $k_{p,ML}$ (d⁻¹), were computed through trapezoidal integration of $k_{p,z}$ over time (3 h intervals) and depth (between the surface and the MLD), followed by division by the MLD.

Global $k_{\rm p,z}$ fields were computed at $1^{\circ} \times 1^{\circ}$ horizontal resolution (Fig. 2), to which all input variables had been previously regridded. Mixed-layer photolysis rates, $P_{\rm ML}$ (nmol L^{-1} d⁻¹), were computed as the product of monthly $1^{\circ} \times 1^{\circ}$ fields of $k_{\rm p,ML}$ and sea-surface DMS concentration (nmol L^{-1}) (Hulswar et al. 2022), assuming constant DMS in the UML. Gridded $P_{\rm ML}$ fields were finally integrated over different spatiotemporal domains (Table 1).

Detailed information on the input data and the optical submodels used to compute the factors in Eq. 4 and generate the associated intermediate datasets is provided in the Supporting Information Data S1-S3. Briefly, a global monthly climatology of $E_{d,0-}(\lambda)$ at 3 h sub-daily resolution was computed using the atmospheric radiative transfer code SBDART (Ricchiazzi et al. 1998), as described by Laliberté et al. (2016); $K_{\rm d}(\lambda)$ was computed using the SeaUV algorithm (Cao et al. 2014) from a monthly climatology of remote sensing reflectance spectra (SeaWiFS sensor); $a_{CDOM}(\lambda)$ was computed with the model of Swan et al. (2013); μ_d was computed following Kirk (1991). Note that, instead of a spectral μ_{dr} we used a broadband μ_d centered at 330 nm using as inputs the K_d and the total absorption and scattering coefficients at 330 nm estimated from pre-established bio-optical relationships. Additional analyses were performed to ensure consistency between the various optical submodels (Supporting Information Data S2). We assessed uncertainty by altering the input variables with Gaussian noise (Supporting Information Data S3). Our calculations and the figures shown in the main article and SM can be reproduced with the code and datasets provided in a public repository (Galí et al. 2022), which requires Matlab® 2010b or later.

Pre-existing parameterizations

PAR-normalized photolysis rate constant

The spectrally resolved model was compared with a simpler parameterization, named KO_SCALED . In this scheme $k_{p,z}$ is proportional to broadband visible irradiance, hereafter called photosynthetically available radiation (PAR):

$$k_{\rm p,z} = k^{\rm PAR} \, {\rm PAR}_{\rm 0-} \cdot \exp(-K_{\rm d}(490) \cdot z)$$
 (eq5)

where $k^{\rm PAR}$ is a rate constant normalized to PAR that takes a fixed value with units of [d⁻¹ (irradiance)⁻¹]. Here, we computed PAR₀— as the spectral integral of SBDART outputs between 400 and 700 nm, and vertical PAR attenuation using $K_{\rm d}$ at 490 nm from SeaUV.

This approach was employed in early DMS models (Vézina 2004) and later adopted in some global models (Bopp et al. 2008; Vogt et al. 2010) with varying $k^{\rm PAR}$ values. Here, we set $k^{\rm PAR}=0.0128~{\rm m}^2~({\rm mol~photons})^{-1}$, the median of 111 globally distributed measurements of $k_{\rm p,0-}$ divided by their corresponding SBDART-derived PAR₀₋ (Galí et al. 2016). This value facilitates comparisons between KO_SCALED and the spectral models $CDOM_NO3$ and $CDOM_SST$, derived from the same dataset. Alternative PAR-dependent formulations used in the PISCES model family, based on Belviso et al. (2012), are briefly discussed in section 2.2 and analyzed in Supporting Information Data S4.

Fixed photolysis rate constant

We tested an even simpler scheme, named KO_FIXED , that prescribes a fixed $k_{\rm p,0-}$ regardless of subsurface irradiance, and attenuates $k_{\rm p,z}$ following $K_{\rm d}(490)$:

$$k_{p,z} = k_{p,0-}^{C} \exp(-K_d(490) \cdot z)$$
 (eq6)

Following Chu et al. (2003), here we set $k_{p,0-}^{C} = 0.5 \text{ d}^{-1}$.

Results and discussion

Spatiotemporal patterns

According to our model, DMS photolysis removes between 17.5 and 20.0 Tg S yr $^{-1}$ from the UML globally. The lower and upper bounds are obtained, respectively, when AQY(330) is estimated with the empirical parameterizations $CDOM_SST$ (Eq. 1B) or $CDOM_NO3$ (Eq. 1A). Sea-surface photolysis rate constants, $k_{\rm p,0-}$, resulting from these AQY parameterizations agree within $\pm 30\%$ in 50% of the pixels on an annual basis, but differences are larger in the tropical Pacific and the Arctic (Fig. 3e,f). Hence, despite uncertainties in AQY submodels (see section 2.3), the two equations likely provide realistic bounds for the estimation of global DMS photolysis.

Taking the *CDOM_NO3* model as a reference, we obtain a global area-weighted mean $k_{\rm p,0-}$ of 0.44 d⁻¹ (all means reported hereafter are weighted by pixel area). Although the mean $k_{\rm p,0-}$ is higher during the summer, as expected from the seasonal cycle of irradiance, relatively large spatial variations

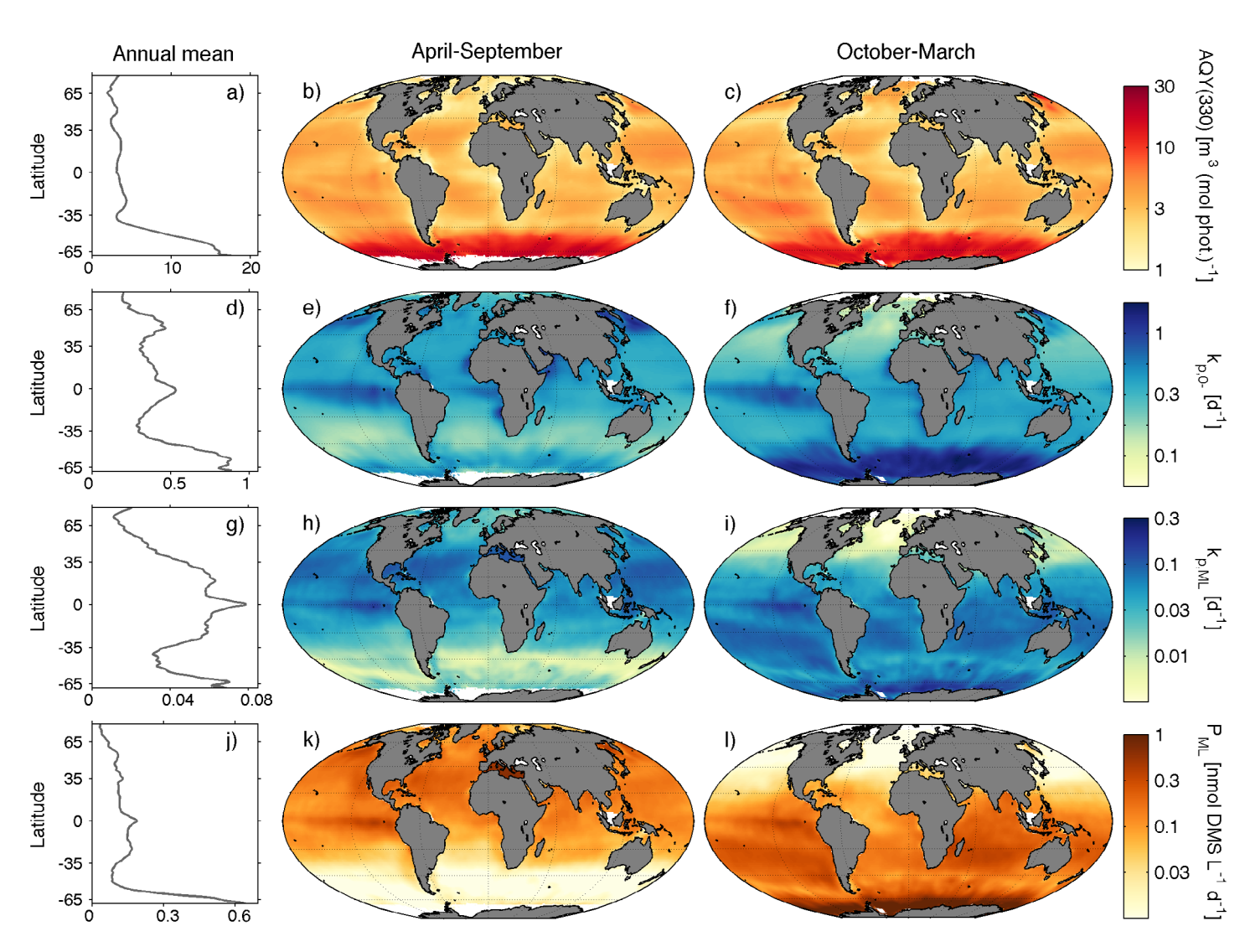


Fig. 2. Global DMS photolysis rates estimated with an empirical model and satellite data: (a-c) DMS photolysis AQY at the reference wavelength, AQY(330); (**d**-**f**) daily mean photolysis rate constants at the sea surface $(k_{p,0-})$; (**g**-**i**) daily mean photolysis rate constants in the UML $(k_{p,ML})$; (**j**-**l**) photolysis rates in the UML. Left panels show the annual zonal averages. Center and right panels show, respectively, the means for the boreal and austral summer semesters centered on the solstices.

Table 1. DMS photolysis rates (Tq S per period) obtained with our spectral model using two alternative parameterizations for the DMS photolysis AQY (CDOM_NO3 and CDOM_SST) and with two simplified parameterizations for the sea-surface photolysis rate constant used in global biogeochemical models.

Model	Northern hemisphere			Southern hemisphere			Global
	Apr–Sep	Oct–Mar	Year	Apr–Sep	Oct–Mar	Year	Year
CDOM_NO3 ^a	3.6	1.8	5.4	2.8	11.7	14.5	20.0
CDOM_SST ^b	3.0	1.3	4.3	2.2	10.9	13.1	17.5
K0_SCALED ^c	10.2	5.9	16.1	9.1	20.0	29.1	45.2
K0_FIXED ^d	9.2	6.9	16.1	11.8	19.5	31.2	47.3

^aEquation 1A: Fit between AQY(330) and a_{CDOM,330} and NO₃⁻.

^bEquation 1B: Fit between AQY(330) and a_{CDOM,330} and SST with an interaction term.

^cEquation 5: $k_{\rm p,z}$ scaled to PAR_z as in Vogt et al. 2010, with modified parameters. ^dEquation 6: fixed $k_{\rm p,0-}$ as in Chu et al. 2003.

are observed, reflecting spatial AQY variability (Fig. 2a–c). Mixed-layer mean rate constants, $k_{\rm p,ML}$ (Fig. 2h,i), show wider seasonality than $k_{\rm p,0-}$ (Fig. 2e,f). This pattern arises from the shoaling of the UML during the summer, itself a result of high solar irradiance, which implies that a larger fraction of the UML experiences high UV exposure, hence bringing $k_{\rm p,ML}$ closer to $k_{\rm p,0-}$.

Mixed-layer photolysis rates (Fig. 2j–l) are calculated from the product of $k_{\rm p,ML}$ and a monthly climatology of sea-surface DMS concentration. Since DMS concentrations peak during the summer and are generally higher in subpolar and polar latitudes, summertime photolysis rates are further intensified at high latitudes in comparison to $k_{\rm p,ML}$. These general patterns hold when the default DMS fields, provided by the most recent climatology (Hulswar et al. 2022), are replaced by the previous climatology (Lana et al. 2011). The older climatology produces slightly lower global DMS photolysis rates (16.8–19.8 Tg S yr⁻¹), despite having 4% higher DMS concentration globally, because of differences in the spatiotemporal DMS distribution.

Meridional asymmetry is the most conspicuous feature in global DMS photolysis rates. Around 73% of the total annual photolysis occurs in the Southern Hemisphere, which accounts for 57% of the ocean area, and ~ 35% occurs south of 40° S, within 21% of the ocean area. This feature has not been reported for other photochemical processes, and results primarily from the high AQYs observed in the Southern Ocean (Toole et al. 2004), which are captured by our statistical models (Figs. 1, 2a–c). High AQYs counteract the prevailing low irradiance in the Southern Ocean (Supporting Information Fig. S4), such that $k_{\rm p,0-}$ south of 40° S are 62% higher than the global average. Deep mixing plays a dual role in the Southern Ocean: it lowers $k_{\rm p,ML}$ to 0.040 d⁻¹, slightly below the global mean of 0.052 d⁻¹, but increases total photolysis because the rates are integrated over a thicker mixed layer.

In our spectral model, vertical attenuation of $k_{\rm p,z}$ is variable by construction. To depict this variability, we computed the linear regression between $\ln(k_{\rm p,z})$ and depth for each pixel and month. The resulting regression slope is $K_{\rm d}(k_{\rm p,z})$, the $k_{\rm p,z}$ vertical attenuation coefficient. Over the first two optical depths, $K_{\rm d}(k_{\rm p,z})$ is generally within $\pm 10\%$ of $K_{\rm d}(330)$ (Supporting Information Fig. S4), and typically ranges between 0.09 and 0.28 m⁻¹ (68% central values). On a global average, the 10% attenuation depth of $k_{\rm p,z}$ is 14.5 m. Thus, DMS photolysis is usually confined in the UML. If we assume that sea-surface $a_{\rm CDOM}$ and AQY can be extrapolated below the UML, and do not truncate photolysis at $z={\rm MLD}$, the integral of $k_{\rm p,z}$ increases by only 9% globally. This result agrees with global models of photochemical processes that show similar spectral dependence (Fichot and Miller 2010; Zhu and Kieber 2020).

Simplified parameterizations: Caveats and potential improvement

Global DMS photolysis estimates based on the schemes *KO_FIXED* and *KO_SCALED*, representative of current

biogeochemical models, exceed our best estimates by more than twofold (Table 1). The main reason for this overestimation is that they attenuate photolysis vertically following PAR rather than UV radiation. Indeed, PAR-dependent $k_{\rm p,z}$ penetrates much deeper in the water column, with an average 10% attenuation depth of 56 m. Consequently, these schemes overestimate photolysis in the UML (Fig. 3b,d), and below it. Also note that, unlike the simplified schemes, our spectral photolysis model is proportional to scalar downwelling irradiance, defined as the quotient between planar irradiance and the mean cosine ($E_{\rm d}/\mu_{\rm d}$). Accounting for $\mu_{\rm d}$ (i.e., the tridimensional light field) in the simplified models would exacerbate their positive bias.

The global average $k_{\rm p,0-}$ simulated with the simplified schemes (0.45-0.50 d⁻¹) and with the CDOM_NO3 scheme (0.44 d⁻¹) are in good agreement. Yet, they show distinct spatial deviations (Fig. 3). Surprisingly, KO_FIXED shows better agreement with the reference fields than KO SCALED in terms of their annual mean $k_{p,0-}$. Indeed, prescribing a fixed $k_{p,0-}$ is unrealistic in extratropical regions with a marked seasonal cycle of irradiance. The KO_SCALED scheme exhibits a positive (negative) deviation at low (high) latitudes, with particularly negative bias in the Southern Ocean. In the Belviso et al. (2012) and subsequent PISCES model versions this spatial bias is corrected by adding a nitrate-dependent photolysis term. However, these newer versions adopted a Michaelis-Menten formulation for both PAR- and nitrate-dependent photolysis. which is not supported by measurements (Kieber et al. 1996; Bouillon and Miller 2004: Toole et al. 2004).

In section Supporting Information Data S4 and Supplementary Table S3 we review the value of $k^{\rm PAR}$ in different models, which determine each model's biases together with PAR forcing fields. Significantly, we found an order-of-magnitude error in the value of the $k^{\rm PAR}$ parameter that apparently creeped from the text of Lefèvre et al. (2002) and Vézina (2004) into, at least, the codes of Bopp et al. (2008) and Vogt et al. (2010). We therefore recommend that future model studies provide more careful descriptions of their parameters and forcing fields.

As a corollary to this subsection, we compare Eqs. 4-6 to analyze and evaluate the implicit assumptions made in each simplified scheme. Whereas, KO_FIXED assumes that the spectral integral $\int E_{d,0-}(\lambda) \cdot a_{CDOM}(\lambda) \cdot AQY(\lambda)$ d λ is constant, the KO_SCALED scheme assumes that only $\int a_{CDOM}(\lambda) \cdot AQY(\lambda) d\lambda$ is constant. For different reasons, none of these assumptions holds when evaluated against our spectral model forced by seasonally varying irradiance. Nevertheless, the KO_SCALED scheme allows for more realistic seasonality and could be readily improved by (i) prescribing spatial k^{PAR} arrays adjusted to match the spectral model outputs, and (ii) empirically correcting the vertical attenuation of $k_{p,z}$, $K_d(k_{p,z})$ (see section 2.1). The latter can be estimated from remotely sensed $K_d(490)$ using this regression equation: $K_d(k_{p,z}) = 1.9854 \cdot [K_d(490)^{1.0713}]$, with $R^2 = 0.83$. This fit provides a direct means to correct $K_d(490)$ in Eq. 5.

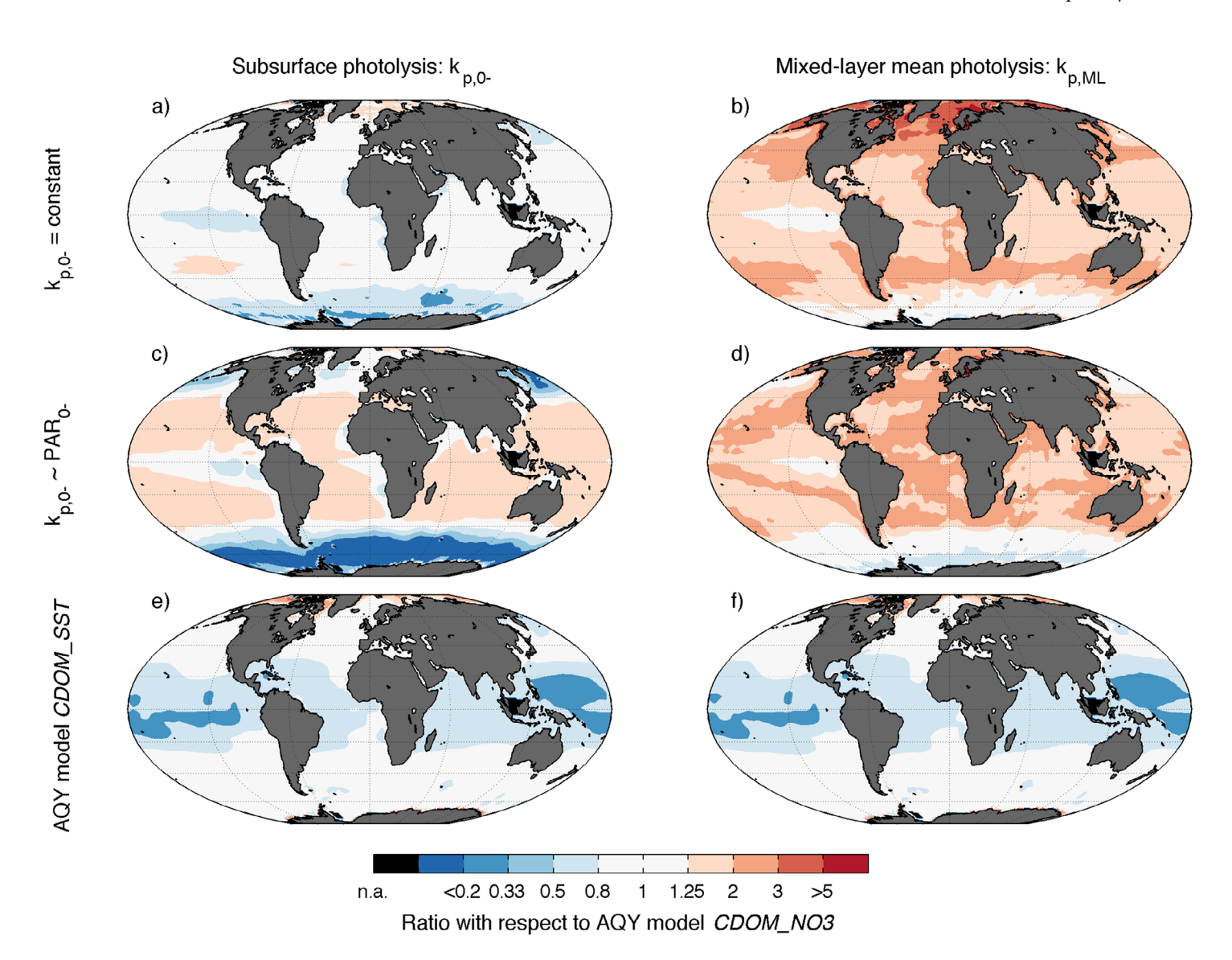


Fig. 3. Comparison between annual mean photolysis rate constants for DMS at the sea surface (left) and the UML (right) obtained with different parameterizations (rows), expressed as their ratio with respect to the reference model (spectral model with AQY as a function of CDOM and NO₃⁻): (**a**, **b**) K0_FIXED model with constant sub-surface photolysis rate constant $k_{p,0-}$; (**c**, **d**) K0_SCALED model with $k_{p,0-}$ proportional to subsurface PAR₀₋; (**e**, **f**) alternative spectral model with AQY as a function of CDOM and SST.

Strengths and limitations of the spectral model

Unlike previous assessments of photochemical processes, which used a fixed AQY spectrum globally (Fichot and Miller 2010; Zhu and Kieber 2020; Zhu et al. 2022), spectrally and vertically resolved DMS photolysis assessments require an additional submodel that accounts for AQY variability. Here, we used two alternative parameterizations developed using insitu datasets that encompass the wide ranges of variability of AQY and its predictors (Supplementary Table S1). These submodels produce similar spatial patterns, particularly in the Southern Ocean high-photolysis area (Fig. 3e,f), suggesting the main findings reported here are robust.

Still, the AQY parameterizations are the largest source of uncertainty in our approach. Smaller uncertainties arise from satellite retrievals and optical modeling as discussed in Supporting Information Data S1–3. Perturbation of AQY(330) with realistic noise, corresponding to a mean absolute percentage error of 70% (Fig. 1), typically causes deviations in $k_{\rm p,0-}$ within a factor of 1.5 around unperturbed estimates (S3, Supporting Information Fig. S5 and Table S2). These deviations are only slightly increased when uncertainty in $S_{\rm AQY}$ (Eq. 3) is accounted for. Whereas random pixel-wise uncertainties tend to cancel out over large spatiotemporal scales, AQY model biases (Fig. 1b) may persist. However, the in-situ

dataset is likely too small to ascertain to what extent sampling and model biases propagate to global estimates.

It is worth noting that, with the aim of maximizing the explained AQY(330) variance, nitrate and SST are used as empirical predictors in Eq. 1A,B. Thus, as discussed by Galí et al. (2016), their coefficients do not reflect their mechanistic effects on AQY(330). New in-situ studies are needed to develop more mechanistic (and eventually more precise) representations of AQY variability. Such studies should consider in greater detail the photosensitizing and radical-scavenging properties of CDOM and other photochemically active substances, temperature effects, and their joint impact on AQY seasonality, which could not be validated in our model.

Concluding remarks

Calculations based on the meta-analysis of in situ data suggested that photolysis was a larger sink for DMS in the UML than emission to the atmosphere (Galí and Simó 2015). However, our results imply that this is not the case but rather that photolysis removes $\sim 30\%$ less DMS than the 27 Tg S yr $^{-1}$ removed by sea-air gas exchange (Hulswar et al. 2022). The bias of in situ sampling toward the summer season likely explains this discrepancy (Galí and Simó 2015). This unexpected conclusion of our study demonstrates the importance of using Earth observation data to extrapolate in situ rates to large scales. Similar techniques can be used for upscaling estimates of biological DMS production and consumption, whose global magnitude is poorly constrained.

Existing biogeochemical models are found to overestimate global DMS photolysis by around 150%, mostly because they prescribe the vertical attenuation of photolysis rates as a function of visible radiation (PAR). In future simulations photolysis should be attenuated as a function of UV radiation, e.g., using the $K_{\rm d}(330)$ or the photolysis spectrum-weighted $K_{\rm d}$ provided here. Model projections should also consider the response of known drivers of DMS photolysis under global change scenarios.

Surface Southern Ocean waters stand out as a DMS photolysis hotspot globally. Notably, the ocean area south of 40° S (21% of the ocean surface) accounts for $\sim\!23\%$ of DMS emission (Hulswar et al. 2022) and $\sim\!35\%$ of DMS photolysis globally. Secondary aerosols derived from atmospheric DMS oxidation play a key role in this region because of the low influence of anthropogenic and terrestrial aerosol sources and the summer minimum in primary marine aerosol (Fiddes et al. 2018; Fossum et al. 2018). Further work is warranted to understand the role of photolysis in controlling DMS emission in this climatically important area.

Data availability statement

The data and code necessary to reproduce the article's results and figures are available in https://doi.org/10.5281/zenodo.7890912.

References

- Belviso, S., and others. 2012. DMS dynamics in the most oligotrophic subtropical zones of the global ocean. Biogeochemistry **110**: 215–241. doi:10.1007/s10533-011-9648-1
- Bock, J., and others. 2021. Evaluation of ocean dimethylsulfide concentration and emission in CMIP6 models. Biogeosciences **18**: 3823–3860. doi:10.5194/bg-18-3823-2021
- Bopp, L., O. Aumont, S. Belviso, and S. Blain. 2008. Modelling the effect of iron fertilization on dimethylsulphide emissions in the Southern Ocean. Deep-Sea Res. II Top. Stud. Oceanogr. **55**: 901–912. doi:10.1016/j.dsr2.2007.12.002
- Bouillon, R.-C., and W. L. Miller. 2004. Determination of apparent quantum yield spectra of DMS photo-degradation in an in situ iron-induced Northeast Pacific Ocean bloom. Geophys. Res. Lett. **31**: L06310. doi:10.1029/2004GL 019536
- Brimblecombe, P., and D. Shooter. 1986. Photo-oxidation of dimethylsulphide in aqueous solution. Mar. Chem. **19**: 343–353. doi:10.1016/0304-4203(86)90055-1
- Cao, F., C. G. Fichot, S. B. Hooker, and W. L. Miller. 2014. Improved algorithms for accurate retrieval of UV/visible diffuse attenuation coefficients in optically complex, inshore waters. Remote Sens. Environ. **144**: 11–27. doi:10. 1016/j.rse.2014.01.003
- Carslaw, K. S., and others. 2013. Large contribution of natural aerosols to uncertainty in indirect forcing. Nature **503**: 67–71. doi:10.1038/nature12674
- Charlson, R. J., J. E. Lovelock, M. O. Andreae, and S. G. Warren. 1987. Oceanic phytoplankton, atmospheric sulphur, cloud albedo and climate. Nature **326**: 655–661. doi: 10.1038/326655a0
- Chu, S., S. Elliott, and M. E. Maltrud. 2003. Global eddy permitting simulations of surface ocean nitrogen, iron, sulfur cycling. Chemosphere **50**: 223–235. doi:10.1016/S0045-6 535(02)00162-5
- Le Clainche, Y., and others. 2010. A first appraisal of prognostic ocean DMS models and prospects for their use in climate models. Global Biogeochem. Cycles **24**: GB3021. doi: 10.1029/2009GB003721
- Fichot, C. G., and W. L. Miller. 2010. An approach to quantify depth-resolved marine photochemical fluxes using remote sensing: Application to carbon monoxide (CO) photoproduction. Remote Sens. Environ. **114**: 1363–1377. doi:10.1016/j.rse.2010.01.019
- Fiddes, S. L., M. T. Woodhouse, Z. Nicholls, T. P. Lane, and R. Schofield. 2018. Cloud, precipitation and radiation responses to large perturbations in global dimethyl sulfide. Atmos. Chem. Phys. **18**: 10177–10198.
- Fossum, K. N., and others. 2018. Summertime primary and secondary contributions to Southern Ocean cloud condensation nuclei. Sci. Rep. **8**: 1–14. doi:10.1038/s41598-018-32047-4

Galí, M., and R. Simó. 2015. A meta-analysis of oceanic DMS and DMSP cycling processes: Disentangling the summer paradox. Global Biogeochem. Cycles **29**: 496–515. doi:10. 1002/2014GB004940

- Galí, M., and others. 2016. CDOM sources and Photobleaching control quantum yields for oceanic DMS photolysis. Environ. Sci. Technol. **50**: 13361–13370. doi:10.1021/acs.est.6b04278
- Galí, M., G. L. Pérez, E. Devred, D. J. Kieber, R. Simó. 2022. Global ocean dimethylsulfide (DMS) photolysis model. Zenodo. doi:10.5281/zenodo.8112739
- Hulswar, S., and others. 2022. Third revision of the global surface seawater dimethyl sulfide climatology (DMS-Rev3). Earth Syst. Sci. Data **14**: 2963–2987. doi:10.17632/hyn62s pny2.1
- Kieber, D. J., J. Jiao, R. P. Kiene, and T. S. Bates. 1996. Impact of dimethylsulfide photochemistry on methyl sulfur cycling in the equatorial Pacific Ocean. J. Geophys. Res. **101**: 3715–3722. doi:10.1029/95JC03624
- Kirk, J. T. O. 1991. Volume scattering function, average cosines, and the underwater light field. Limnol. Oceanogr. **36**: 455–467. doi:10.4319/lo.1991.36.3.0455
- Laliberté, J., S. Bélanger, and R. Frouin. 2016. Evaluation of satellite-based algorithms to estimate photosynthetically available radiation (PAR) reaching the ocean surface at high northern latitudes. Remote Sens. Environ. **184**: 199–211. doi:10.1016/j.rse.2016.06.014
- Lana, A., and others. 2011. An updated climatology of surface dimethlysulfide concentrations and emission fluxes in the global ocean. Global Biogeochem. Cycles **25**: GB1004. doi: 10.1029/2010GB003850
- Lefèvre, M., A. Vézina, M. Levasseur, and J. W. H. Dacey. 2002. A model of dimethylsulfide dynamics for the subtropical North Atlantic. Deep. Res. Part I Oceanogr. Res. Pap. **49**: 2221–2239. doi:10.1016/S0967-0637(02) 00121-8
- Ricchiazzi, P., S. Yang, C. Gautier, and D. Sowle. 1998. SBDART: A research and teaching software tool for plane-parallel radiative transfer in the Earth's atmosphere. Bull. Am. Meteorol. Soc. **79**: 2101–2114. doi:10.1175/1520-0477 (1998)079<2101:SARATS>2.0.CO;2
- Schmidtko, S., G. C. Johnson, and J. M. Lyman. 2013. MIMOC: A global monthly isopycnal upper-ocean climatology with mixed layers. J. Geophys. Res. Ocean. **118**: 1658–1672. doi:10.1002/jgrc.20122
- Shaw, G. E. 1983. Bio-controlled thermostasis involving the sulfur cycle. Clim. Change **5**: 297–303. doi:10.1007/BF0 2423524
- Swan, C. M., N. B. Nelson, D. A. Siegel, and E. A. Fields. 2013. A model for remote estimation of ultraviolet absorption by chromophoric dissolved organic matter based on the global distribution of spectral slope. Remote Sens. Environ. 136: 277–285. doi:10.1016/j.rse.2013. 05.009

- Tesdal, J.-E., J. R. Christian, A. H. Monahan, and K. von Salzen. 2016. Evaluation of diverse approaches for estimating seasurface DMS concentration and air-sea exchange at global scale. Environ. Chem. **13**: 390–412. doi:10.1071/EN14255
- Toole, D. A., D. J. Kieber, R. P. Kiene, D. A. Siegel, and N. B. Nelson. 2003. Photolysis and the dimethylsulfide (DMS) summer paradox in the Sargasso Sea. Limnol. Oceanogr. **48**: 1088–1100. doi:10.4319/lo.2003.48.3.1088
- Toole, D. A., D. J. Kieber, R. P. Kiene, E. M. White, J. Bisgrove, D. A. del Valle, and D. Slezak. 2004. High dimethylsulfide photolysis rates in nitrate-rich Antarctic waters. Geophys. Res. Lett. **31**: L11307. doi:10.1029/2004GL019863
- Toole, D. A., D. Slezak, R. P. Kiene, D. J. Kieber, and D. A. Siegel. 2006. Effects of solar radiation on dimethylsulfide cycling in the western Atlantic Ocean. Deep-Sea Res. I Oceanogr. Res. Pap. **53**: 136–153.
- del Valle, D., D. J. Kieber, D. A. Toole, J. Brinkley, and R. P. Kiene. 2009. Biological consumption of dimethylsulfide (DMS) and its importance in DMS dynamics in the Ross Sea, Antarctica. Limnol. Oceanogr. **54**: 785–798.
- Vézina, A. F. 2004. Ecosystem modelling of the cycling of marine dimethylsulfide: A review of current approaches and of the potential for extrapolation to global scales. Can. J. Fish. Aquat. Sci. **61**: 845–856. doi:10.1139/F04-025
- Vogt, M., S. M. Vallina, E. T. Buitenhuis, L. Bopp, and C. Le Quéré. 2010. Simulating dimethylsulphide seasonality with the dynamic Green Ocean model PlankTOM5. J. Geophys. Res. **115**: 1–21. doi:10.1029/2009JC005529
- Yang, M., S. D. Archer, B. W. Blomquist, D. T. Ho, V. P. Lance, and R. J. Torres. 2013. Lagrangian evolution of DMS during the Southern Ocean gas exchange experiment: The effects of vertical mixing and biological community shift. J. Geophys. Res. Ocean. 118: 6774–6790. doi:10.1002/2013JC009329
- Zhai, X., Y. C. Song, J. L. Li, J. Yang, H. H. Zhang, and G. P. Yang. 2020. Distribution characteristics of Dimethylated sulfur compounds and turnover of Dimethylsulfide in the northern South China Sea during summer. J. Geophys. Res. Biogeo. **125**: 1–14. doi:10.1029/2019JG005363
- Zhu, Y., and D. J. Kieber. 2020. Global model for depth-dependent carbonyl photochemical production rates in seawater. Global Biogeochem. Cycles **34**: e2019GB006431. doi:10.1029/2019GB006431
- Zhu, Y., L. C. Powers, D. J. Kieber, and W. L. Miller. 2022. Depth-resolved photochemical production of hydrogen peroxide in the global ocean using remotely sensed ocean color. Front. Remote Sens. 3: 1–17. doi:10.3389/frsen.2022.1009398

Acknowledgments

We thank the NASA Ocean Biology Distributed Active Archive Center (OB. DAAC) for access to satellite data, Maxime Benoît-Gagné for guidance with radiative transfer computations and the Takuvik Joint International Laboratory (CNRS-France and Univeristé Laval-Canada) for access to computing facilities. MG received funding from a Beatriu de Pinós postdoctoral fellowship (2013 BP-A 00098, AGAUR, Generalitat de Catalunya) and the project DMS-Cons (PIE 202230I123, Spanish Govern-

ment). RS received funding from the European Research Council (ERC) under the European Union's Horizon 2020 research and innovation programme (Project ERC-2018-AdG Grant Agreement No. 834162). The Institute of Marine Sciences (ICM-CSIC) is supported by a "Severo Ochoa" Centre of Excellence grant (CEX2019-000928-S) from the Spanish government. We thank two anonymous reviewers for their constructive comments.

Conflict of Interest

None declared.

Submitted 21 October 2022 Revised 04 May 2023 Accepted 09 June 2023